Pharm Res (2017) 34:1683–1692
DOI 10.1007/s11095-017-2165-8

RESEARCH PAPER

A Functional Iron Oxide Nanoparticles Modified with PLA-PEG-DG as Tumor-Targeted MRI Contrast Agent

Fei Xiong[1,2] • Ke Hu[1,2] • Haoli Yu[1,2] • Lijun Zhou[3] • Lina Song[1,2] • Yu Zhang[1,2] • Xiuhong Shan[4] • Jianping Liu[4] • Ning Gu[1,2]

Received: 21 January 2017 / Accepted: 25 April 2017 / Published online: 12 June 2017

ABSTRACT

Purpose Tumor targeting could greatly promote the performance of magnetic nanomaterials as MRI (Magnetic Resonance Imaging) agent for tumor diagnosis. Herein, we reported a novel magnetic nanoparticle modified with PLA (poly lactic acid)-PEG (polyethylene glycol)-DG (D-glucosamine) as Tumor-targeted MRI Contrast Agent.

Methods In this work, we took use of the D-glucose passive targeting on tumor cells, combining it on PLA-PEG through amide reaction, and then wrapped the PLA-PEG-DG up to the Fe_3O_4@OA NPs. The stability and anti phagocytosis of Fe_3O_4@OA@PLA-PEG-DG was tested in vitro; the MRI efficiency and toxicity was also detected in vivo.

Results These functional magnetic nanoparticles demonstrated good biocompatibility and stability both in vitro and in vivo. Cell experiments showed that Fe_3O_4@OA@PLA-PEG-DG nanoparticles exist good anti phagocytosis and high targetability. In vivo MRI images showed that the contrast effect of Fe_3O_4@OA@PLA-PEG-DG nanoparticles prevailed over the commercial non tumor-targeting magnetic nanomaterials MRI agent at a relatively low dose.

Conclusions The DG can validly enhance the tumor-targetting effect of Fe_3O_4@OA@PLA-PEG nanoparticle. Maybe MRI agents with DG can hold promise as tumor-targetting development in the future.

KEY WORDS contrast agent · D-glucosamine · Fe_3O_4 NPs · MRI · tumor targeting

ABBREVIATIONS

^{18}F–FDG	[^{18}F] fluoro-2-deoxy-D-glucose
DG	D-glucosamine
GLUT1	Glucose transporters 1
NPs	Nanoparticles
PEG	Polyethylene glycol
PLA	Poly lactic acid
SPIONs	Superparamagnetic iron oxide nanoparticles

INTRODUCTION

Anticancer Therapies has been widely used in cancer therapy over the last 6 decades [1]. One of their main defects is that these anticancer drugs cannot precisely target tumor cells within the pathologic sites, which weakens their anticancer effects and causes severe toxic and side effects [2–5]. A promising approach to overcome these limitations is to covalently conjugate drugs to a targeting ligand which can specifically bind to the tumor cells [6–9]. Glucose, which plays a significant role in human physiology, is an essential energy source in the process of metabolism. Malignant tumors show an enhanced glycolytic rate and a high demand of glucose, even under

Electronic supplementary material The online version of this article (doi:10.1007/s11095-017-2165-8) contains supplementary material, which is available to authorized users.

✉ Fei Xiong
xiongfei@seu.edu.cn

✉ Ning Gu
guning@seu.edu.cn

1 State Key Laboratory of Bioelectronics, Jiangsu Laboratory for Biomaterials and Devices, School of Biological Science and Medical Engineering, Southeast University, Nanjing 210096, China

2 Collaborative Innovation Center of Suzhou Nano-Science and Technology, Suzhou Key Laboratory of Biomaterials and Technologies, Suzhou 215123, China

3 Institute of Pharmaceutics, China Pharmaceutical University, Nanjing 210096, China

4 Department of Radiology The Affiliated Renmin Hospital, Jiangsu University, Zhenjiang, China

aerobic conditions [10, 11]. It is reported that glucose transporters 1 (GLUT1) is the main mediator of glucose uptake [12]. Accordingly, the increased demand for glucose to supplement energy production in tumors turns into enhanced expression and activity of GLUT1, which can be utilized as targeting ligand for drugs [13, 14]. GLUT1 activity in mammalian cells has been monitored by radiolabeled tracers such as [^{18}F] fluoro-2-deoxy-D-glucose (^{18}F–FDG), [^{14}C] 2-deoxy-D-glucose, and [^{14}C] or [^{3}H] 3-O-methyl-D- glucose [15–18]. ^{18}F–FDG is the most common radiotracer of increased glucose metabolism to visualize tumor activity and location with positron emission tomography (PET) in the clinical settings. The method is sensitive and quantitative [15, 19]. However, ^{18}F–FDG is impractical owing to the short half-life of the isotope for many high throughput preclinical studies. Besides, radiolabeled tracers often exist radiotoxicity to human organs. Therefore, it is worthwhile to alter to D-glucosamine (DG) labeled imaging agents.

Magnetic resonance imaging (MRI) is a powerful medical diagnostic imaging technique for soft tissue imaging among the imaging modalities [20]. Other advantages of MRI include nonionizing radiation, multiplanar imaging capability, the MRI images are high sensitively and specificity, permitting in depth anatomical details in the diagnosis of many diseases [21]. Superparamagnetic iron oxide nanoparticles (SPIONs, Fe_3O_4 or γ- Fe_3O_4) are one of the most adopted magnetic nanoprobes for T2 weighted MRI studies [22]. However, SPIONs in circulation are generally susceptible to opsonization which induces their instability and specific uptake by the reticuloendothelial system (RES) prior to reaching the target tissue, leading to a significant reduction in efficiency in diagnostics and therapeutics based on nanoparticles [23–25]. It has been demonstrated that PEGylation was a useful strategy to minimize the biofouling and aggregation of SPIONs in physiological conditions due to the hydrophilicity and steric repulsion of PEG chains [26–30].

In previous, we have reported functionalized NPs as magnetic nanoprobe targeting on tumor cells and obtained good effects [21]. In this paper, a novel Fe_3O_4@Oleic acid (OA) @poly lactic acid (PLA) - polyethylene glycol (PEG)-DG was developed. These DG-modified nanoparticles provided higher magnetic responses than the summation of the single ones, indicating better MRI effect. Besides, thanks to the stable interaction between Fe_3O_4@OA NPs and PLA-PEG-DG, Fe_3O_4@OA@PLA-PEG-DG NPs were bestowed a high ability to resist phagocytosis by macrophages in vitro. Furthermore, the studies on the in vivo behavior of Fe_3O_4@OA@PLA-PEG-DG NPs revealed their good performance in tumor imaging at a relatively low dose.

EXPERIMENTAL SECTION

Materials and Characterization

All reagents and solvents were obtained from commercial suppliers and were used without further purification. PLA-PEG (6 k, 2 k) was purchased from Shanghai Jing Yu Biotechnology Co., Ltd. 1-(3-Dimethylaminopropyl)-3-ethylcarbodiimide hydrochloride (EDC·HCl) was purchased from Shanghai Shao Yuan Chemical Co., Ltd. N-Hydroxysuccinimide (NHS) was purchased from Shanghai Medpep Co., Ltd. Dulbecco's modified eagle medium (DMEM) was purchased from Gibco. Note that DMEM used in our experiments contains 10% (*V*/V) fetal bovine serum. Superparamagnetic Fe_3O_4 nanoparticles capped with oleic acid (Fe_3O_4@OA NPs) were prepared via the coprecipitation method according to literature [29]. The iron contents of the Fe_3O_4@OA NPs were determined by the colorimetric method using *o*-phenanthroline. FT-IR spectra were performed on a Model VECTOR FT-IR spectrometer (Bruker Co., Germany). Transmission electron microscopic (TEM) analysis was carried out on a JEM-2000EX microscope (JEOL Co., Japan). Thermogravimetric Analysis (TGA) analyses were carried out with a Pyris 1 TGA analyzer (PerKinElmer Co., USA) at a heating rate of 20°C per min under a nitrogen atmosphere. Dynamic Light Scattering (DLS) experiments were run on a 90 Plus Nanoparticle Size Analyzer (Brookhaven Instruments Co., USA) in the 90° backscattering mode. The zeta potential of the samples was obtained with Zetaplus (Brookhaven Instruments Co., USA). Magnetic properties were determined with vibrating sample magnetometer (VSM, Lakeshore 7407) at room temperature in a field up to 10 kOe. The r2 relaxivity was measured in a 1.5 T Eclipse MR imager (Philip Co., Netherlands). The following pulse sequence was used fast spin echo with TR = 5500 ms, TE = 101 ms, echo train length (ET) =16 ms. The FOV was set at 14 cm × 14 cm with NEX = 2–4.

Synthesis of the PLA-PEG-DG

PLA-PEG (25.3 mg) was dissolved in 2 mL Dimethylformamide (DMF) and 6 mL water. After 3 h standing at room temperature, EDC·HCl (550 mg), NHS (370 mg) were added to the reaction system and the resulting mixture was stirred for 20 min at room temperature. Then, DG (350 mg) was added to the reaction system and the resulting mixture was stirred for12h at room temperature [31]. Thereafter, the resulting mixture was purified by dialysis against water for 24 h to removal organic solvents. The solution of PLA-PEG-DG was obtained by the filtration of microporous filtering films with 0.22 μm for degerming.

Synthesis of the Fe3O4@OA@PLA-PEG-DG NPs

Fe_3O_4@OA NPs (20 mg) was dissolved in 4 ml Tetrahydrofuran (THF) after magnetic adsorption separation using 2 ml ethyl alcohol (EtOH). After ultrasonic oscillato, PLA-PEG-DG (20 mg) was added to the reaction system and the resulting mixture was ultrasonic oscillated for 5 min. Thereafter, the resulting mixture was added into water drop by drop, and ultrasonic oscillated for 3 min (Power = 750 W, Pulse on: 2 s, Pulse off: 2 s) [32]. The resulting mixture was purified by dialysis against water for 24 h to removal organic solvents. The solution of Fe_3O_4@OA@PLA-PEG-DG NPs was obtained by the filtration of microporous filtering films with 0.22 μm for degerming.

In Vitro Cytotoxicity

The RAW 264.7 macrophages and 4 T1 cell line were used to measure the in vitro cytotoxicity of Fe_3O_4@OA@PLA-PEG-DG NPs. An amount of 10^4 RAW 264.7 macrophages and 4 T1 cells were plated in each well of 96-well plates overnight and co-incubated with series of concentrations of Fe_3O_4@OA @PLA-PEG-DG NPs at 37°C for 24 h, respectively. Thereafter, the nanoparticles were replaced with 100 μl of fresh culture medium containing 10 μl CCK-8, and the cells were incubated for a further 4 h at 37°C. After cooling to room temperature, the cells were measured using a Microplate Reader (Bio-Rad Co., USA) at 450 nm. Cell viability was expressed as percentage of absorbance in comparison with that of the control, which comprised the cells without exposure to the samples.

Nanoparticles Cell Uptake

Raw 264.7 macrophages and 4 T1 cells were cultured in each well of 24-well plates with 10^4 cells per well, respectively. To compare the unspecific uptake, Resovist, Fe_3O_4@OA@PLA-PEG NPs, Fe_3O_4@OA @PLA-PEG-DG NPs were added in a final concentration of 20, 50 or 100 μg/mL per well. After 12 h, each well was washed with PBS 3 times, treated with 0.5 mL of 4% paraformaldehyde solution for 20 min to fix the cells, and then washed with PBS, stained successively by Prussian blue for ferric ions and nuclear fast red for cell nucleus, and examined by optical microscopy. Meanwhile, to quantitatively determine the amount of Fe_3O_4@OA NPs inside cells the intracellular amount of iron was examined, using a JEM-2100 scanning UV-visible range spectrophotometer (JEOL Co, Japan).

In Vivo MR Imaging

All animal experiments were performed in compliance with guidelines set by the Animal Care Committee of the Southeast University. To establish the experimental model of the tumor, 4 T1 cells (2×10^6 cells per mouse) were inoculated subcutaneously into the proximal thigh region of BABL mice (18-22 g). MR images were taken prior to the injection of the Fe_3O_4@OA NPs samples and at appropriate time points post injection. Mice were anesthetized for imaging with isoflurane (1.5% vol. at 2 L min^{-1}) via a nose cone. Body temperature was maintained at 37°C. Physiological saline, Resovist, Fe_3O_4@OA@PLA-PEG NPs and Fe_3O_4@OA@PLA-PEG-DG NPs in saline solutions were injected intravenously through the tail vein, respectively. Three mice were examined for each Fe_3O_4@OA NPs sample. The in vivo MRI experiments were performed under the same experiment conditions with the use of a 3 cm circular surface coil in transmit/receive mode conducting on 7 Tesla Micro-MRI (PharmaScan, BrukersBioSpin MRI Co., Germany). MR imaging of mice was performed with T_2* flash sequence. The parameters were TR/TE = 3000 ms/40 ms, flip angle = 180°, FOV = 40 mm × 40 mm, slice thickness = 1 mm, matrix 256 × 256.

Histology Study

At 2 h after the injection of physiological saline, Resovist, Fe_3O_4@OA@PLA-PEG NPs and Fe_3O_4@OA@PLA-PEG-DG NPs, the tumor tissues from the mice were dissected and fixed in 10% neutral buffered formalin. The tissues were processed routinely into paraffin, sectioned at a thickness of 4 μm, stained successively by Prussian blue for ferric ions and nuclear fast red for cell nucleus, and examined by optical microscopy.

Vascular Stimulation Test

Vascular irritation test of Fe_3O_4@OA@PLA-PEG-DG NPs was performed by intravenous injection in rabbits, (1.85 mg/kg, and one time per day for three days) with physiological saline as control. Three rabbits were examined for each group. Injection parts were observation by naked eyes 48-96 h after the last injection. Thereafter, the ears from the rabbit were dissected and fixed in 10% neutral buffered formalin. The tissues were processed routinely into paraffin, stained successively by hematoxylin-eosin (HE) and examined by optical microscopy.

Acute Toxicological Test

Acute Toxicological Test of Fe_3O_4@OA@PLA-PEG-DG NPs was carried out by intravenous injection in mice, (4 mg Fe/kg, and one time per day for three days) with physiological saline as control. Five mice were examined for each group. The mice were killed 24 h post-injection. Liver and kidneys were dissected and fixed in 10% neutral buffered formalin. The tissues were processed routinely into paraffin and examined by optical microscopy.

All the animal experiments were performed in compliance with the Guidelines of the Animal Research Ethics Board of Southeast University. Full details of approval of the study can be found in the approval ID: 20,080,925.

RESULTS AND DISCUSSION

Synthesis and Characterization of the PLA-PEG-DG

After the activation of the carboxylic groups on PLA-PEG with EDC·Cl and NHS, D- glucosamine is linked to PLA-PEG via amidation reaction with large excess of D- glucosamine. The covalent linkage of D- glucosamine to PLA-PEG was confirmed by the FT-IR spectrometry (Fig. 1a) and measurement of D-glucosamine, using Elson-Morgan method (Fig. 1b). Apart from the IR absorption peak at 1758 cm^{-1}, characteristic of the carboxylic carbonyl groups in PLA-PEG (C = O stretching), the FT-IR spectrum of PLA-PEG-DG exhibits a peak at 1699 cm^{-1} that can be assigned to the amide carbonyl groups, indicating the successful linkage of D- glucosamine to the surface of PLA-PEG via amidation reaction. Additionally, absorption bands at 3297 cm^{-1} and 1600 cm^{-1}, which are attributable to the stretching and bending vibration of amino bond of PLA-PEG-DG, respectively. Accordingly, the results of FT-IR demonstrate explicitly the formation of PLA-PEG-DG.

The amounts of DG on the PLA-PEG were assessed by Elson-Morgan method [33] (Fig. 1b). DG was determined at 527 nm. As shown in Fig. 1b, the concentration of D-glucosamine has good linearity between 4 ~ 24 μg/ml. The reactants EDC, NHS and PLA-PEG have no ultraviolet absorption at 525 nm, which means they did not interfere with the determination. According to calculations, the purity of the synthetic product is 97.99%.

Synthesis and Characterization of Fe3O4@OA@PLA-PEG-DG NPs

The preparation of the Fe_3O_4@OA@PLA-PEG-DG NPs is shown schematically in Scheme 1. After magnetic separation, Fe_3O_4@OA NPs were dissolved in THF-where PLA-PEG-DG was added. Thereafter, the resulting mixture was added into water drop by drop, and ultrasonic oscillated. The hydrophobic ends of PLA-PEG-DG and the OA layers of the Fe_3O_4 NPs attached together through hydrophobic interaction. Meanwhile the hydrophilic ends stretch in the water, achieving th.e scattering of oil soluble iron oxide into water steadily. The resulting mixture was purified by dialysis against water for 24 h to removal organic solvents. The solution of Fe_3O_4@OA@PLA-PEG-DG NPs was obtained by the filtration of microporous filtering films with 0.22 μm for degerming.

The linkage of PLA-PEG-DG to Fe_3O_4@OA NPs was confirmed by the FT-IR spectrometry (Fig. 2a), In the spectrum of Fe_3O_4@OA NPs, the strong absorption peek at 1685 cm^{-1} and weak absorption peek at 1531 cm^{-1} belong to the dissymmetrical (v_{as}) and symmetrical (v_s) stretching vibration peak of carboxylic carbonyl groups, which means that a covalent bond formed between oleic acid and iron core. The bond is linked at the surface of the iron core, which can prevent the iron core from aggregating. The absorption peek at 594 cm^{-1} belongs to the characteristic absorption peak of the magnetic iron oxide core. In contrast with Fe_3O_4@OA NPs, the strong absorption peek at 1111 cm^{-1} of the spectrum Fe_3O_4@OA@PLA-PEG-DG NPs belongs to the

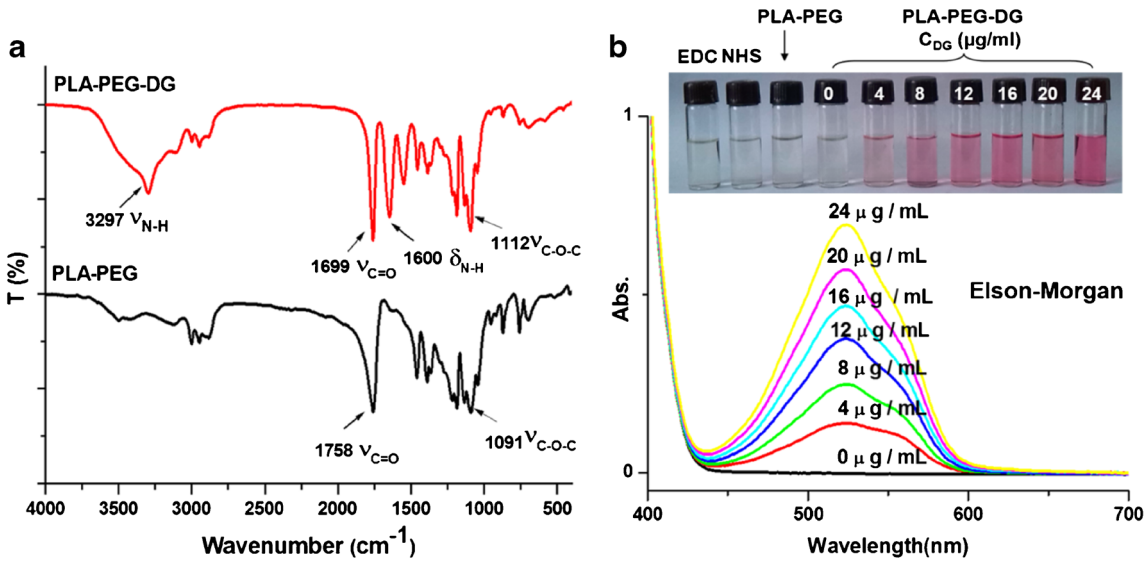

Fig. 1 (**a**) FT-IR spectra of PLA-PEG and PLA-PEG-DG and (**b**) photos and absorption curves of DG solutions of different concentration after the Elson-Morgan reaction.

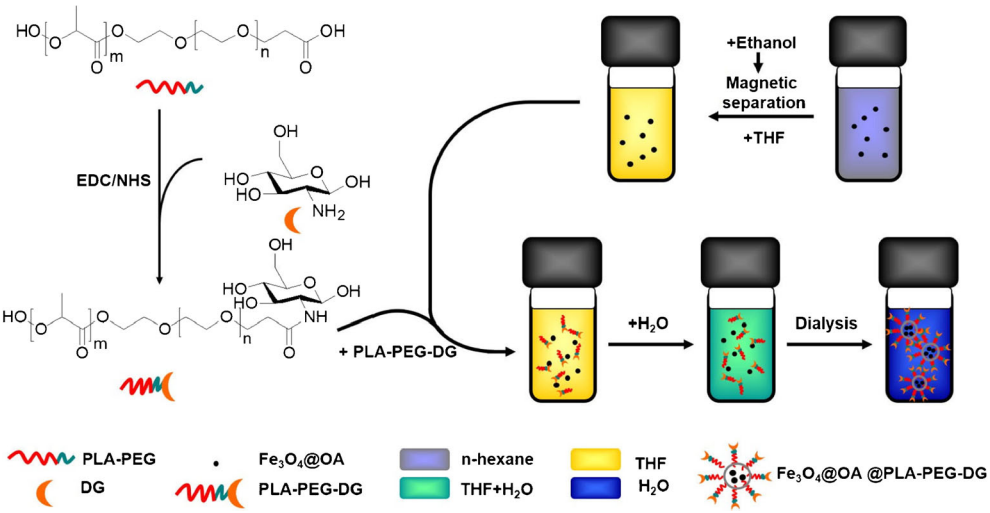

Scheme 1 Schematic diagrams of the preparation of Fe_3O_4@OA@PLA-PEG-DG NPs.

characteristic absorption peak of $–CH_2$-O-CH_2-. The broad absorption peek at 3441 cm^{-1} belongs to the stretching vibration peek of amino N-H ($\nu_{N\text{-}H}$), and the absorption peek at 1601 cm^{-1} belongs to the bending vibration peek of amide N-H ($\delta_{N\text{-}H}$). Based on the results above, it shows that PLA-PEG-DG has been decorated on the surface of Fe_3O_4@OA NPs.

The amounts of PLA-PEG-DG on the Fe_3O_4@OA NPs were assessed by Thermal Gravimetric Analyzer (TGA) (Fig. 2b). From room temperature to 700°C, the percentage of decrease in mass of Fe_3O_4@OA NPs and Fe_3O_4@OA@PLA-PEG-DG NPs is 32% and 92%, respectively. From room temperature to 400°C, the downtrend of both is similarly 30% approximately. That is because the oleic acid of the system is volatile on heating. When the temperature is above 400°C, the mass loss of Fe_3O_4@OA NPs flattens, while Fe_3O_4@OA @PLA-PEG-DG NPs, with higher content of amphiphilic copolymer, still remains massive decline in mass (~71%). Then the loss flattens. Based on the results of TGA, it can be calculated that the amount of PLA-PEG-DG on Fe_3O_4@OA NPs is 1.51 mmol/g Fe_3O_4. This PLA-PEG-DG density has demonstrated to be high enough to stabilize the Fe_3O_4@OA NPs in physiological conditions and to be used for tumor targeting [34].

The morphological structure of Fe_3O_4@OA NPs and Fe_3O_4@OA@PLA-PEG-DG NPs was analyzed by transmission electron microcopy (TEM, Fig. 2c,d). Fe_3O_4@OA has good monodispersity, the mean diameter of the particles is 5 ~ 6 nm approximately from TEM. Fe_3O_4@OA@PLA-PEG-DG NPs exists as nanocluster, whose diameter is 20 ~ 40 nm approximately in average. The research shows that these magnetic particles of nanocluster exhibit more responsive to the external magnetic field, and also have greater relaxation rate [35–37].

The placement stability of Fe_3O_4@OA@PLA-PEG-DG NPs was investigated with hydrodynamic diameter and Zeta potential as evaluation indexes. The hydrodynamic diameter was studied by DLS and Zeta potential was studied by measuring the Zeta potentials. In 7 days, the hydrodynamic diameter of Fe_3O_4@OA@PLA-PEG-DG NPs is (62.7 ± 2.3) nm evenly, polydispersity index is 0.107, and Zeta potential is (−26.53 ± 2.28) mV. This notes the particles exhibit excellent stability. In order to verify the successful modification of DG, the hydrodynamic diameter and Zeta potential of Fe_3O_4@OA@PLA-PEG NPs and PLA-PEG-DG was measured equally. Fe_3O_4@OA@PLA-PEG NPs provided (64.1 ± 1.7)nm of hydrodynamic diameter and (−30.15 ± 2.76)mV of Zeta potential, as well as PLA-PEG-DG providing (20.5 ± 1.0)nm and (−17.21 ± 2.06)mV. In contrast with magnetic nanoparticles decorated with poly(lactic-co-gycolic acid) (PLGA), PLL, the diameter of Fe_3O_4@OA @PLA-PEG-DG NPs is smaller, which range from 1 to 100 nm, thus it may avoid be phagocytized by the RES [38, 39].

For clinical application as an MRI contrast agent, it is critical that Fe_3O_4@OA NPs retain their magnetic properties after the modification treatments. The magnetic properties of Fe_3O_4@OA@PLA-PEG-DG NPs were investigated by using a vibrating sample magnetometer (VSM) (Fig. 2e). As expected, these Fe_3O_4@OA @PLA-PEG-DG NPs are superparamagnetic at room temperature and the hysteresis loops show negligible hysteresis. The saturation magnetization values of Fe_3O_4@OA@PLA-PEG-DG NPs is 57.79eum/g Fe at 25°C (Fig. 2e), suggesting that the decoration has little influence on the superparamagnetism of Fe_3O_4@OA NPs.

RAW 264.7 Macrophages Phagocytosis Experiment of the Fe3O4@OA@PLA-PEG-DG NPs

To assess the ability of Fe_3O_4@OA@PLA-PEG-DG NPs to escape RES uptake, RAW 264.7 macrophages phagocytosis experiments were conducted as a prelude for in vivo studies. After the incubation with Resovist (a clinical approved

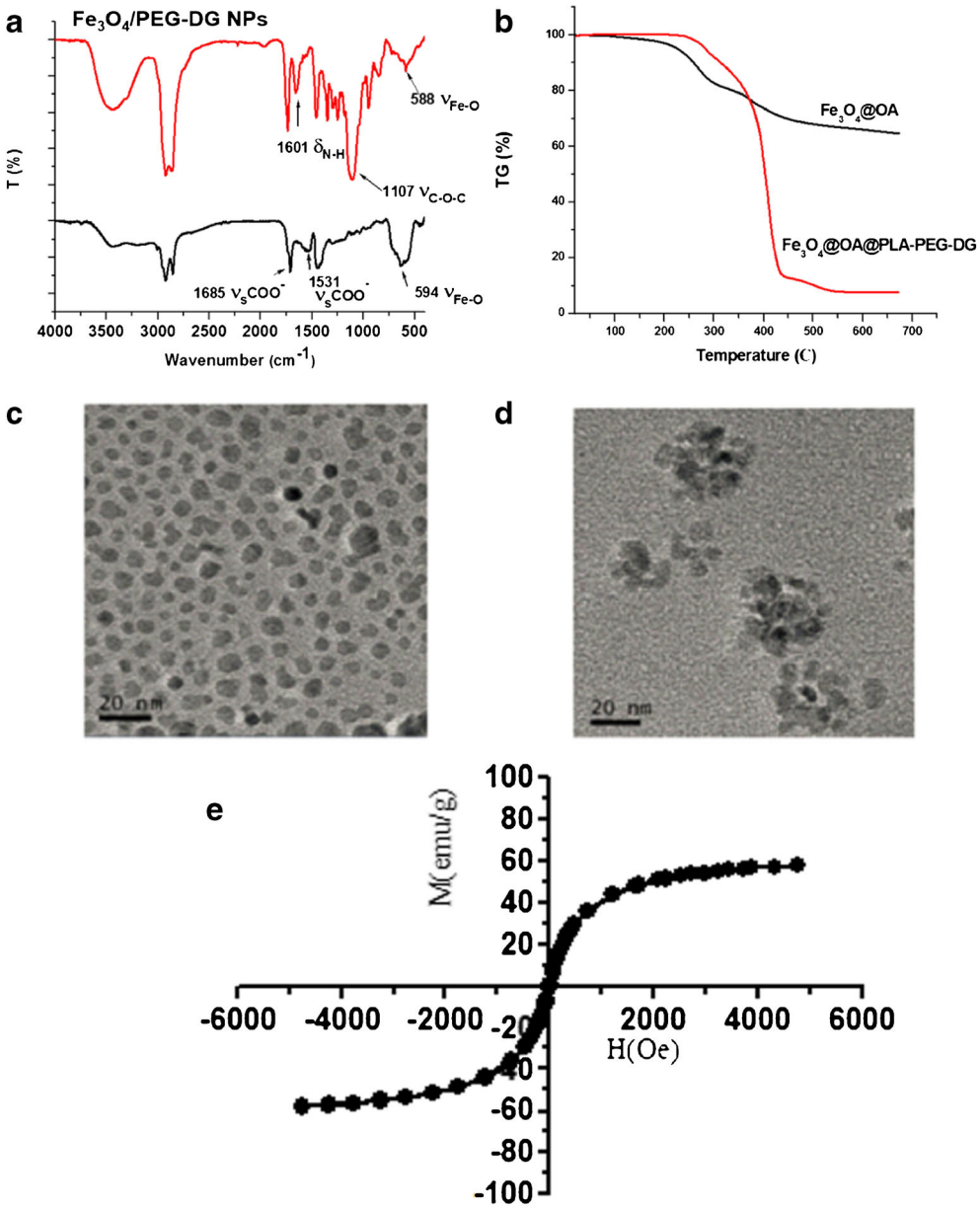

Fig. 2 (**a**) FT-IR spectrums of Fe_3O_4@OA NPs and Fe_3O_4@OA@PLA-PEG-DG NPs. (**b**) Thermogravimetric analysis of Fe_3O_4@OA NPs and Fe_3O_4@OA @PLA-PEG-DG NPs. (**c**) Transmission electron micrograph of Fe_3O_4@OA NPs. (**d**) Transmission electron micrograph of Fe_3O_4@OA@PLA-PEG-DG NPs. (**e**) Hysteresis loops at room temperature for Fe_3O_4@OA NPs and Fe_3O_4@OA @PLA-PEG-DG NPs. (M: magnetization value; H: magnetic field strength).

SPION-based MRI contrast agent), Fe_3O_4@OA@PLA-PEG NPs, and Fe_3O_4@OA@PLA-PEG-DG NPs for 12 h and washing with PBS, the macrophages were stained with Prussian blue to qualitatively determine the amount of Fe_3O_4@OA NPs inside cells (Fig. 3). It can be observed that most of the macrophages incubated with Resovist are stained blue, indicating that the Resovist can be readily phagocytized by macrophages and would remain mostly in the cytoplasm. In marked contrast, no blue color can be detected in the cells incubated with Fe_3O_4@OA@PLA-PEG NPs, and Fe_3O_4@OA @PLA-PEG-DG NPs and subsequently stained with Prussian blue, indicating that Fe_3O_4@OA@PLA-PEG NPs and Fe_3O_4@OA@PLA-PEG-DG NPs both can avoid being swallowed by macrophages effectively, and have potential stealth long circulating action.

4 T1 Cells Uptake Experiment of the Fe3O4@OA@PLA-PEG-DG NPs

To further assess the active targeting effect on tumor cells of Fe_3O_4@OA @PLA-PEG-DG NPs in vitro, 4 T1 cell uptake experiments were carried out. After the incubation with Fe_3O_4@OA@PLA-PEG NPs and Fe_3O_4@OA@PLA-PEG-DG NPs for 2 h and washing with PBS, the 4 T1 cells were stained with Prussian blue to qualitatively determine the amount of Fe_3O_4@OA NPs inside cells (Fig. 4). As shown in Fig. 4, Fe_3O_4@OA@PLA-PEG-DG NPs was significantly phagocytized, while no conspicuous phagocytosis of Fe_3O_4@OA@PLA-PEG NPs observed, which indicates that the uptake of Fe_3O_4@OA @PLA-PEG-DG NPs by 4 T1 cells is due to the DG decorated on the nanoparticles. On the other

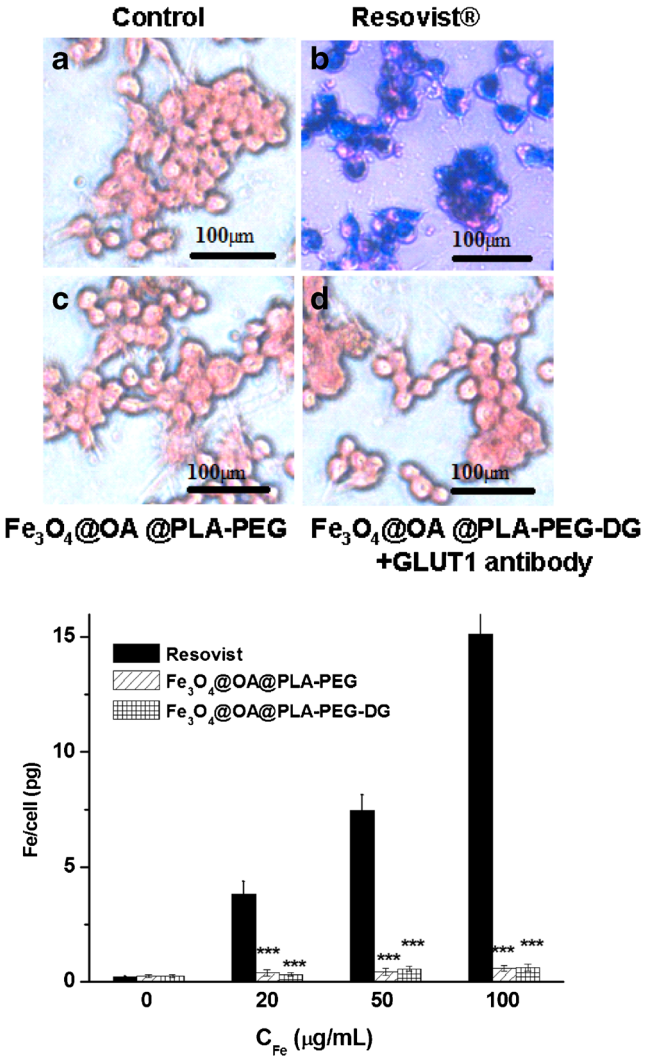

Fig. 3 In vitro Prussian blue staining images of macrophages RAW264.7 treated with 100 μg Fe/mL of (**a**) Control (**b**) Resovist, (**c**) Fe_3O_4@OA@PLA-PEG NPs and d) Fe_3O_4@OA@PLA-PEG-DG NPs for 12 h.

hand, the uptake is significantly decrease after pretreated with GLUT1 antibody, which further demonstrates that the uptake is induced by GLUT1. Depend on the results above, we may arrive at the conclusion that Fe_3O_4@OA@PLA-PEG-DG NPs have certain active targeting effect on tumor cells in vitro, and increase the specific uptake of tumor cells in vitro.

In Vivo MRI and Biodistribution of the Fe3O4@OA@PLA-PEG-DG

In order to further assess the application potentials of Fe_3O_4@OA@PLA-PEG-DG NPs in cancer imaging by MRI, its in vivo performance was investigated. Tumor-bearing mice were prepared by subcutaneous injection of 4 T1 cells into their proximal thigh region. To evaluate the in vivo performance of Fe_3O_4@OA@PLA-PEG-DG NPs more clearly, physiological saline, Fe_3O_4@OA @PLA-PEG

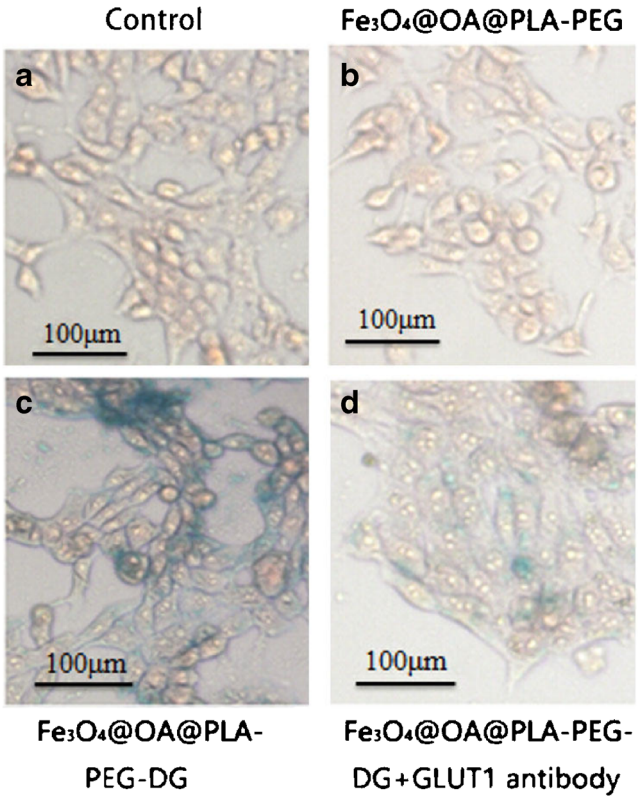

Fig. 4 In vitro Prussian blue staining images of 4 T1 cells of control and 12 h treatment with 100 μg Fe/mL, of Fe_3O_4@OA@PLA-PEG NPs, Fe_3O_4@OA@PLA-PEG-DG NPs and Fe_3O_4@OA@PLA-PEG-DG NPs with cells pretreated with GLUT1 antibody for 2 h.

NPs and Resovist were examined in parallel as references. The saline solutions of Fe_3O_4@OA@PLA-PEG NPs, Fe_3O_4@OA@PLA-PEG-DG NPs and Resovist were injected via tail vein with the dose of 4 mg Fe per kilogram body weight. The dose of Fe_3O_4@OA NPs used in our experiments is comparatively lower than that used in recently published works [39–41]. The T_2*-weighted MR images of the mice were record at scheduled temporal points pre- and post-injection. For the mice treated with Fe_3O_4@OA@PLA-PEG-DG NPs, a significant decrease of the signal intensity in tumor area is observed at 2 h post-injection (Fig. 5a,b). The relative MRI signal decrease (RSD, %) in the region of interests (ROIs, as indicated by the white arrows) of tumor was calculated to be 64.61 ± 7.34% compared with pre-injection, revealing a massive accumulation of the Fe_3O_4@OA NPs in the tumor. For the mice treated with Fe_3O_4@OA@PLA-PEG NPs, the RSD values in ROIs of tumor were calculated to be 21.64 ± 3.78%, which significantly smaller ($P < 0.05$) than that of the mice group treated with Fe_3O_4@OA@PLA-PEG-DG NPs. For the two mouse groups treated with physiological saline and Resovist, no significant changes in tumor tissues were found at 2 h post-injection under the injected dose (Fig. 5a,b). Based on the MRI analyses, it is reasonable to say that the Fe_3O_4@OA@PLA-PEG-DG NPs have much higher ability

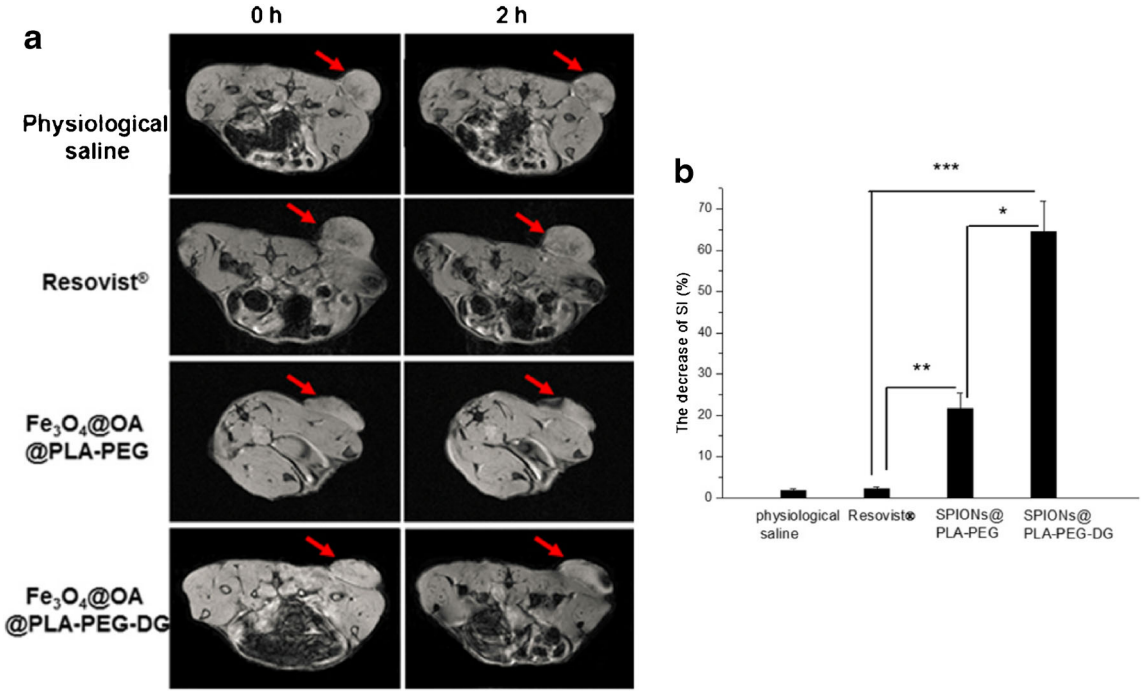

Fig. 5 (**a**) T2*-weighted images at pre-injection and 2 h post-injection of 4 mg Fe/Kg of a) physiological saline, (**b**) Resovist (**c**) Fe_3O_4@OA@PLA-PEG NPs and (**d**) Fe_3O_4@OA@PLA-PEG-DG NPs in the regions of the tumor on the proximal thigh of the BABL/c mice. b) The signal intensity (SI) decrease at 2 h post-injection of 4 mg Fe/Kg of physiological saline, Resovist, Fe_3O_4@OA@PLA-PEG NPs and Fe_3O_4@OA@PLA-PEG-DG NPs in the regions of the tumor on the proximal thigh of the BABL/c mice. Results were shown as mean ± SD (n = 3).

to accumulate in tumor tissue than Fe_3O_4@OA@PLA-PEG NPs and Resovist, which is attributed to the specific targeting effect of DG. Another point worth mentioning is that, the dose of contrast agent we injected in mice is below the reported ones, with greater RSD value, which indicates that the Fe_3O_4@OA @PLA-PEG-DG NPs we made not only has the ability of tumor targeting, but also shows greater responding ability to the external magnetic field and larger relaxation rate, which lead to lower T_2*signal intensity, and better contrast effect [40–42]. As active targeting contrast agent, Fe_3O_4@OA@PLA-PEG-DG NPs should have great application foreground.

To further verify the MRI results and confirm the existence of Fe_3O_4@OA @PLA-PEG-DG NPs in tumor tissues. Liver, spleen and tumor slices were resected at 2 h after the injection of physiological saline, Fe_3O_4@OA@PLA-PEG NPs and Resovist, the slices were stained successively by Prussian blue for ferric ions and nuclear fast red solution for cell nucleus, and then the slices were analyzed via optical microscopy. As shown in Fig. 6, Resovist gathered largely at liver, slightly at spleen and hardly at tumor tissues, consistent with the reported literature. Meanwhile, Fe_3O_4@OA@PLA-PEG NPs and Fe_3O_4@OA@PLA-PEG-DG NPs gathered slightly at liver and spleen, significantly smaller than Resovist group, which indicates that both Fe_3O_4@OA@PLA-PEG NPs and Fe_3O_4@OA@PLA-PEG-DG NPs could avoid being uptake by mononuclear macrophage, which have reverse passive targeting effect. Fe_3O_4@OA@PLA-PEG-DG NPs gathered significantly at tumors, clearly larger than Resovist group,

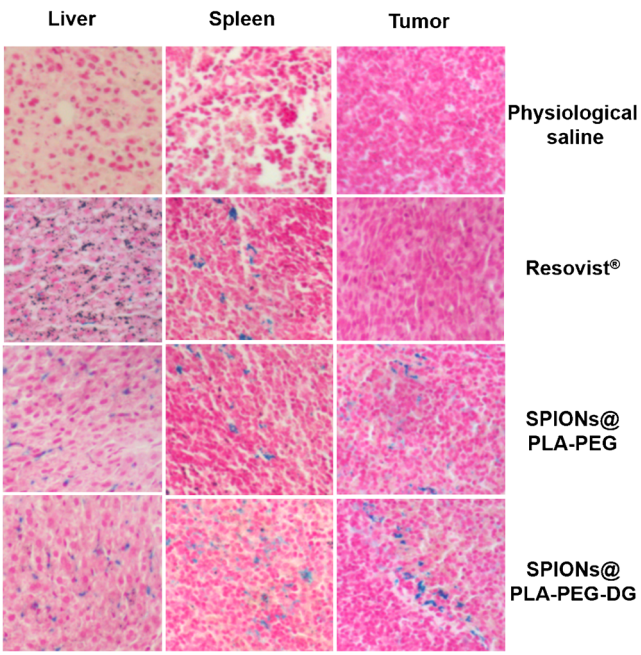

Fig. 6 Ex vivo Prussian blue and nuclear fast red double staining images of tissues excised from BABL/c mice at 2 h post-injection of 4 mg Fe/mL of physiological saline, Resovist, Fe_3O_4@OA@PLA-PEG NPs and Fe_3O_4@OA@PLA-PEG-DG NPs.

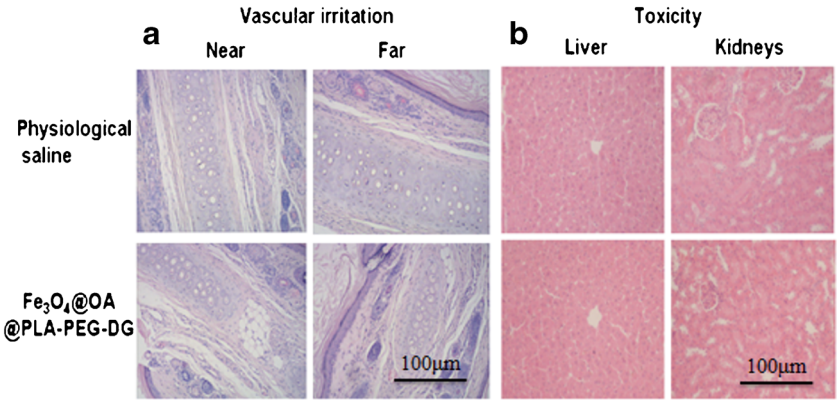

Fig. 7 (**a**) Vascular stimulation test (near: 1.3 cm from the needle point, far: 4.0 cm from the needle point) (**b**) toxicity tests of Fe_3O_4@OA@PLA-PEG-DG NPs.

which means Fe_3O_4@OA NPs decorated by DG exhibit great active targeting effect. This result is consistent with the in vivo MR image analyses.

Vascular Stimulation and Toxicity Tests of Fe3O4@OA @PLA-PEG-DG NPs

It was necessary to evaluate the toxicity of Fe_3O_4@OA @PLA-PEG-DG NPs, since they would eventually be used in living body as MRI contrast agent. Vascular stimulation test was performed by intravenous injection in rabbits at a dose of 1.85 mg/kg. As shown in Fig. 7a, 96 h after injection, no bleeding, thrombosis, blood vessel hyperemia, and inflammatory cell infiltrates were found. Toxicity test was carried out by intravenous injection in mice at a dose of 4 mg Fe/kg. As shown in Fig. 7b, no pathological changes were found in liver or kidneys 24 h post-injection. These results suggest that the Fe_3O_4@OA@PLA-PEG-DG NPs prepared by this approach could be applied as a safe MRI contrast agent.

CONCLUSIONS

In conclusion, a novel Fe_3O_4@OA @PLA-PEG-DG NPs as tumor-targeted MRI contrast agent was developed. Characterizations showed that Fe_3O_4@OA@PLA-PEG-DG NPs were of good stability and biocompatibility. The in vitro and in vivo experiments demonstrated that Fe_3O_4@OA@PLA-PEG-DG NPs exhibited high resistance to phagocytosis by macrophages in vitro, and uptaked by the RES in vivo. This endowed the Fe_3O_4@OA with high efficiency in tumor imaging by MRI at a relatively low dose, which prevailed over the commercial non tumor-targeting magnetic nanomaterials MRI agent. These excellent properties resulted from the active targeting effect of the DG. Taken together, the Fe_3O_4@OA@PLA-PEG-DG NPs exhibit great potential application as MRI contrast agents for tumor imaging.

Acknowledgments and Disclosures. This work was financially supported by National Natural Science Foundation of China (81473160), the Basic Research Program of Jiangsu Province (Natural Science Foundation, No. BK20151422 and BK20151334), Scientific and Technological Project of Zhenjiang (No. SS2015023). This work was also sponsored by Qing Lan Project. The authors declare no competing financial interest.

Author Contributions

The manuscript was written through contributions of all authors. All authors have given approval to the final version of the manuscript.

REFERENCES

1. Emmenegger U, Kerbel RS. CANCER chemotherapy counteracted. Nature. 2010;468(7324):637–8.
2. Perrino C, Schiattarella GG, Magliulo F, Ilardi F, Carotenuto G, Gargiulo G, Serino F, Ferrone M, Scudiero F, Carbone A, Trimarco B, Esposito G. Cardiac side effects of chemotherapy: state of art and strategies for a correct management. Curr Vasc Pharmacol. 2014;12(1):106–16.
3. Kim J, Sung N, Raghavendran HB, Yoon Y, Song B, Choi J, Yoo Y, Byun M, Hwang Y, Lee J. Gamma irradiation reduces the immunological toxicity of doxorubicin, anticancer drug. Radiat Phys Chem. 2009;78(7–8):425–8.
4. Raschi E, Vasina V, Ursino MG, Boriani G, Martoni A, De Ponti F. Anticancer drugs and cardiotoxicity: insights and perspectives in the era of targeted therapy. Pharmacol Ther. 2010;125(2):196–218.
5. Pathania D, Millard M, Neamati N. Opportunities in discovery and delivery of anticancer drugs targeting mitochondria and cancer cell metabolism. Adv Drug Deliv Rev. 2009;61(14):1250–75.
6. Kievit FM, Wang FY, Fang C, Mok H, Wang K, Silber JR, Ellenbogen RG, Zhang M. Doxorubicin loaded iron oxide nanoparticles overcome multidrug resistance in cancer *in vitro*. J. Control. Release 2011;152(1SI):76–83.
7. Zhang H, Li F, Yi J, Gu C, Fan L, Qiao Y, Tao Y, Cheng C, Wu H. Folate-decorated maleilated pullulan-doxorubicin conjugate for active tumor-targeted drug delivery (vol 42, pg 517, 2011). Eur J Pharm Sci. 2011;43(5):409.

8. Zheng C, Xu J, Yao X, Xu J, Qiu L. Polyphosphazene nanoparticles for cytoplasmic release of doxorubicin with improved cytotoxicity against dox-resistant tumor cells. J Colloid Interface Sci. 2011;355(2):374–82.
9. Cho H, Yoon I, Yoon HY, Koo H, Jin Y, Ko S, Shim J, Kim K, Kwon IC, Kim D. Polyethylene glycol-conjugated hyaluronic acid-ceramide self-assembled nanoparticles for targeted delivery of doxorubicin. Biomaterials. 2012;33(4):1190–200.
10. Warburg O. Origin of cancer cells. Science. 1956;123(3191): 309–14.
11. Ganapathy V, Thangaraju M, Prasad PD. Nutrient transporters in cancer: relevance to Warburg hypothesis and beyond. Pharmacol. Ther. 2009;121(1):29–40.
12. Hediger MA, Rhoads DB. Molecular physiology of sodium-glucose cotransporters. Physiol Rev. 1994;74(4):993–1026.
13. Amann T, Maegdefrau U, Hartmann A, Agaimy A, Marienhagen J, Weiss TS, Stoeltzing O, Warnecke C, Schoelmerich J, Oefner PJ, Kreutz M, Bosserhoff AK, Hellerbrand C. GLUT1 expression is increased in hepatocellular carcinoma and promotes tumorigenesis. Am J Pathol. 2009;174(4):1544–52.
14. Wellberg EA, Johnson S, Finlay-Schultz J, Lewis AS, Terrell KL, Sartorius CA, Abel ED, Muller WJ, Anderson SM. The glucose transporter GLUT1 is required for ErbB2-induced mammary tumorigenesis. Breast Cancer Res. 2016;18:131.
15. Tabouret-Viaud C, Botsikas D, Delattre BM, Mainta I, Amzalag G, Rager O, Vinh-Hung V, Miralbell R, Ratib O. PET/MR in breast cancer. Semin Nucl Med. 2015;45(4):304–21.
16. Turkheimer F, Moresco RM, Lucignani G, Sokoloff L, Fazio F, Schmidt K. The use of spectral-analysis to determine regional cerebral glucose-utilization with positron emission tomography and [F-18] Fluorodeoxyglucose - theory, implementation, and optimization procedures. J Cerebr Blood F Met. 1994;14(3):406–22.
17. Dienel GA, Cruz NF, Adachi KJ, Sokoloff L, Holden JE. Determination of local brain glucose level with [C-14]methylglucose: effects of glucose supply and demand. Am. J. Physiol. Endoc. M. 1997;273(5):E839–49.
18. Axelrod JD, Pilch PF. Unique Cytochalasin-B binding characteristics of the hepatic glucose carrier. Biochemistry-US. 1983;22(9): 2222–7.
19. Schmidt KC, Lucignani G, Sokoloff L. Fluorine-18-fluorodeoxyglucose PET to determine regional cerebral glucose utilization: A re-examination. J Nucl Med. 1996;37(2):394–9.
20. Jin Y, Jia C, Huang S, O'Donnell M, Gao X. Multifunctional nanoparticles as coupled contrast agents. Nat Commun. 2010;1:41.
21. Xiong F, Zhu Z, Xiong C, Hua X, Shan X, Zhang Y, Gu N. Preparation, characterization of 2-deoxy-D-glucose functionalized Dimercaptosuccinic acid-coated Maghemite nanoparticles for targeting tumor cells. Pharm Res-Dordr. 2012;29(4):1087–97.
22. Bakhtiary Z, Saei AA, Hajipour MJ, Raoufi M, Vermesh O, Mahmoudi M. Targeted superparamagnetic iron oxide nanoparticles for early detection of cancer: possibilities and challenges. Nanomed-Nanotechnol. 2016;12(2):287–307.
23. Pankhurst QA, NTK T, Jones SK, Dobson J. Progress in applications of magnetic nanoparticles in biomedicine. J. Phys. D Appl. Phys. 2009;42(22)
24. Berry CC, Curtis A. Functionalisation of magnetic nanoparticles for applications in biomedicine. J Phys D Appl Phys. 2003;36: R198–206.
25. Moghimi SM, Hunter AC, Murray JC. Long-circulating and target-specific nanoparticles: theory to practice. Pharmacol Rev. 2001;53(2):283–318.
26. Tromsdorf UI, Bruns OT, Salmen SC, Beisiegel U, Weller H. A highly Effective, nontoxic T-1 MR contrast agent based on Ultrasmall PEGylated iron oxide nanoparticles. Nano Lett. 2009;9(12):4434–40.
27. Amstad E, Gillich T, Bilecka I, Textor M, Reimhult E. Ultrastable iron oxide nanoparticle colloidal suspensions using dispersants with catechol-derived anchor groups. Nano Lett. 2009;9(12):4042–8.
28. Amstad E, Zurcher S, Mashaghi A, Wong JY, Textor M, Reimhult E. Surface functionalization of single superparamagnetic iron oxide nanoparticles for targeted magnetic resonance imaging. Small. 2009;5(11):1334–42.
29. Lee H, Lee E, Kim DK, Jang NK, Jeong YY, Jon S. Antibiofouling polymer-coated superparamagnetic iron oxide nanoparticles as potential magnetic resonance contrast agents for *in vivo* cancer imaging. J Am Chem Soc. 2006;128(22):7383–9.
30. Liu D, Wu W, Ling J, Wen S, Gu N, Zhang X. Effective PEGylation of iron oxide nanoparticles for high performance *In Vivo* cancer imaging. Adv Funct Mater. 2011;21(8):1498–504.
31. Shan X, Yuan D, Xiong F, Gu N, Wang P. 2-deoxy-D-glucose modified supermagnetic iron oxide nanoparticles enhance the contrasting effect on MRI of human lung adenocarcinoma A549 tumor in nude mice. Zhonghua Zhong Liu Za Zhi. 2014;36(2):85–91.
32. Chen F, Zhao T, Chen Q, Han L, Fang S, Chen Z. Synthesis and release behavior of methotrexate from Fe3O4/PLA-PEG core/shell nanoparticles with high saturation magnetization. Mater Lett. 2013;108:179–82.
33. Amstad E, Zurcher S, Mashaghi A, Wong JY, Textor M, Reimhult E. Surface functionalization of single superparamagnetic iron oxide nanoparticles for targeted magnetic resonance imaging. Small. 2009;5(11):1334–42.
34. Ai H, Flask C, Weinberg B, Shuai X, Pagel MD, Farrell D, Duerk J, Gao JM. Magnetite-loaded polymeric micelles as ultrasensitive magnetic-resonance probes. Adv Mater. 2005;17(16):1949.
35. Kim J, Lee JE, Lee SH, Yu JH, Lee JH, Park TG, Hyeon T. Designed fabrication of a multifunctional polymer nanomedical platform for simultaneous cancer-targeted imaging and magnetically guided drug delivery. Adv Mater. 2008;20(3):478.
36. Qiu P, Jensen C, Charity N, Towner R, Mao C. Oil phase evaporation-induced self-assembly of hydrophobic nanoparticles into spherical clusters with controlled surface chemistry in an oil-in-water dispersion and comparison of behaviors of individual and clustered iron oxide nanoparticles. J Am Chem Soc. 2010;132(50): 17724–32.
37. Okassa LN, Marchais H, Douziech-Eyrolles L, Herve K, Cohen-Jonathan S, Munnier E, Souce M, Linassier C, Dubois P, Chourpa I. Optimization of iron oxide nanoparticles encapsulation within poly(D,L-lactide-co-glycolide) sub-micron particles. Eur J Pharm Biopharm. 2007;67(1):31–8.
38. Arbab AS, Bashaw LA, Miller BR, Jordan EK, Lewis BK, Kalish H, Frank JA. Characterization of biophysical and metabolic properties of cells labeled with superparamagnetic iron oxide nanoparticles and transfection agent for cellular MR imaging. Radiology. 2003;229(3):838–46.
39. Park J, Yu MK, Jeong YY, Kim JW, Lee K, Phan VN, Jon S. Antibiofouling amphiphilic polymer-coated superparamagnetic iron oxide nanoparticles: synthesis, characterization, and use in cancer imaging *in vivo*. J Mater Chem. 2009;19(35):6412–7.
40. Kim J, Kim HS, Lee N, Kim T, Kim H, Yu T, Song IC, Moon WK, Hyeon T. Multifunctional uniform nanoparticles composed of a magnetite nanocrystal Core and a mesoporous silica Shell for magnetic resonance and fluorescence imaging and for drug delivery. Angew Chem Int Edit. 2008;47(44):8438–41.
41. Liu D, Wu W, Ling J, Wen S, Gu N, Zhang X. Effective PEGylation of iron oxide nanoparticles for high performance *In Vivo* cancer imaging. Adv Funct Mater. 2011;21(8):1498–504.
42. Zheng WM, Gao F, Gu HC. Magnetic polymer nanospheres with high and uniform magnetite content. J Magn Magn Mater. 2005;288:403–10.